Cell

A Nonapoptotic Cell Death Process, Entosis, that Occurs by Cell-in-Cell Invasion

Michael Overholtzer,[1] Arnaud A. Mailleux,[1] Ghassan Mouneimne,[1] Guillaume Normand,[1] Stuart J. Schnitt,[3] Randall W. King,[1] Edmund S. Cibas,[2] and Joan S. Brugge[1,*]
[1]Department of Cell Biology, Harvard Medical School
[2]Department of Pathology, Brigham and Women's Hospital and Harvard Medical School
[3]Department of Pathology, Beth Israel Deaconess Medical Center and Harvard Medical School
Boston, MA 02115, USA
*Correspondence: joan_brugge@hms.harvard.edu
DOI 10.1016/j.cell.2007.10.040

SUMMARY

Epithelial cells require attachment to extracellular matrix (ECM) to suppress an apoptotic cell death program termed anoikis. Here we describe a nonapoptotic cell death program in matrix-detached cells that is initiated by a previously unrecognized and unusual process involving the invasion of one cell into another, leading to a transient state in which a live cell is contained within a neighboring host cell. Live internalized cells are either degraded by lysosomal enzymes or released. We term this cell internalization process entosis and present evidence for entosis as a mechanism underlying the commonly observed "cell-in-cell" cytological feature in human cancers. Further we propose that entosis is driven by compaction force associated with adherens junction formation in the absence of integrin engagement and may represent an intrinsic tumor suppression mechanism for cells that are detached from ECM.

INTRODUCTION

In multicellular organisms, cell proliferation and cell death are carefully coordinated to control the number and organization of cells in tissues and organs. In humans, an imbalance in these processes can result in diseases such as cancer that arises from the accumulation of cells due to hyperproliferation and reduced cell death. Much attention has been focused on apoptosis as a critical cell death mechanism due to its central role in cell clearance during development and also in tumor suppression (Jacobson et al., 1997). However, increasing evidence indicates that nonapoptotic cell death processes are also important physiological modes of cell death (Lockshin and Zakeri, 2004). Nonapoptotic death mechanisms can occur concomitantly with apoptosis or can function as alternative processes when apoptosis is impaired to mediate such important developmental processes as interdigital cell death and hollowing of the mammary ducts during puberty (Chautan et al., 1999; Debnath et al., 2005; Degterev et al., 2005; Mailleux et al., 2007).

Within the mammary gland, an important regulator of epithelial cell survival is attachment to a protein-rich basement membrane or extracellular matrix (ECM). Cell death induced by detachment from ECM functions as a luminal clearing mechanism during development (Mailleux et al., 2007) and also may function as a barrier to the development of carcinomas, which display luminal filling as a hallmark. One form of detachment-induced death is an apoptotic program termed anoikis that has been characterized in suspension cell cultures (Frisch and Francis, 1994; Meredith et al., 1993). Although anoikis likely acts as a barrier to tumor formation or metastasis, its inhibition is unlikely to be sufficient for long-term survival of tumor cells away from ECM, as we have found that nonapoptotic cell clearance mechanisms can compensate for apoptotic defects in detached cell populations (Debnath et al., 2002; Mailleux et al., 2007). Thus, tumors arising in glandular epithelia, such as breast tumors, that display filling of luminal spaces as a hallmark must likely overcome both apoptotic and nonapoptotic cell death programs for long-term survival in the absence of attachment to the basement membrane.

Here we describe a nonapoptotic cell death process that occurs in human tumors and that is provoked by loss of attachment to matrix. This cell death mechanism is initiated by an unusual process involving the invasion of one live cell into another, followed by the degradation of internalized cells by lysosomal enzymes. We term this cell internalization process entosis and provide evidence for entosis in human tumors as a mechanism underlying the "cell-in-cell" or "cannibalism" cytological feature.

RESULTS

MCF10A Cells Internalize into Their Neighbors following Detachment

In tracking the fate of human mammary epithelial MCF10A cells in suspension cultures, we noted that some cells in small aggregates appeared to be inside of large vacuoles, suggesting that they were internalized within a neighboring cell (Figure S1). To further investigate these structures, cells were labeled with green or red fluorescent CellTracker dyes and mixed together in suspension. Internalized cells highlighted by these dyes were observed as early as 6 hr in suspension (Figure 1Aa). Analysis by confocal microscopy demonstrated the complete internalization of one cell within another (Figure 1Ab and Movie S1A) or, in some cases, one cell within a cell that was within a third cell (Figures 1Ac and 1Ad). Cell internalization was also analyzed by immunostaining cytospin preparations of suspended cultures for β-catenin to highlight the plasma membrane. Internalizing cells were observed by 6 hr and comprised approximately 25% of the culture by 12 hr (Figure 1C). To further examine whether cells could be completely internalized into their neighbors, suspended cells were assayed for protection from surface biotinylation. After 12 hr, 18.5% ± 2% of internalizing cells (determined by β-catenin staining) were protected from surface labeling with biotin, indicating their complete internalization (Figure S2).

To examine this process in real time, MCF10A cells in suspension were analyzed by time-lapse microscopy. Cell internalization was initiated approximately 3–6 hr after detachment and took several hours to complete (Figure 1B and Movies S1B and S1C). In some cases, complex structures resulting from several reiterative internalization events were formed (Figure 1Bb), and some cells appeared to reside in a large vacuole following internalization (Figures 1B and S1). Internalizing cells appeared to be viable and to bore into outer cells, suggesting that this process might involve the active invasion of one cell into another (see Movies S1B and S1C). Ultrastructural analysis of engulfed cells from 6 hr suspension cultures did not reveal evidence of apoptotic or necrotic features (Figure 1Ae), and internalizing cells appeared to retain mitochondrial membrane potential (Figure S3).

Cell Internalization Occurs Independent of Apoptotic Processes

Recently it was reported that mouse mammary epithelial cells have phagocytic activity toward apoptotic cells (Monks et al., 2005). To examine whether internalization of MCF10A cells following matrix detachment could be a phagocytic response to an apoptotic program, we first tested whether this process was associated with caspase activation. Apoptosis and cell engulfment were quantified by staining suspended cells for activated caspase-3 and β-catenin. Whereas internalizing cells comprised ~25% of the culture by 12 hr, the percentage of cells with activated caspase-3 did not increase until after 24 hr in suspension (Figure 1C). The overexpression of Bcl2 or treatment of cells with the caspase inhibitor ZVAD-FMK also had no effect on cell internalization even though either could inhibit the activation of caspase-3 in suspension or apoptosis following exposure of monolayer cells to UV irradiation (Figures 1C and 1D).

Suspension cultures were further examined for phosphatydilserine (PS) exposure, an eat-me signal that activates phagocytosis of dying cells (Fadok et al., 1992, 2000), by labeling with a fluorescently tagged Annexin V protein that binds to PS. A population of Annexin V-positive cells was detected at early time points in suspension, i.e., 6 and 12 hr; however, the percentages of Annexin positivity (5%–10%) remained much lower than those of cell internalization at these times (15%–25%) (Figure 1E), and there were no partially internalized cells that were positive for Annexin staining (Figure 1E). The addition of PS-liposomes, which can inhibit phagocytosis by overwhelming the PSR (Fadok et al., 1992), also had no effect on cell internalization although they inhibited the uptake of apoptotic Jurkat cells by J774 mouse macrophages (Figure 1F). We also did not observe any engulfment when MCF10A monolayers were incubated with apoptotic Jurkat cells, suggesting that MCF10A cells cannot readily phagocytize apoptotic cells (data not shown). Taken together, these data demonstrate that cell engulfment of MCF10A cells in suspension cultures is not regulated by apoptotic processes and therefore is distinct from phagocytic clearance mechanisms of dying cells.

Cell Engulfment Requires Actin, Myosin II, Rho, and ROCK Activity

To examine whether actin polymerization or myosin II contraction are required for cell engulfment, cells were treated with latrunculin B (LatB), an inhibitor of actin polymerization, or blebbistatin, a myosin II inhibitor. LatB- and blebbistatin-treated cells aggregated into clumps in suspension but rarely internalized, demonstrating a role for actin polymerization and myosin II in cell engulfment (Figure 2A). We next examined whether Rho signaling, which is a critical regulator of actin and myosin II, also plays a role in this process. Rho GTPases, and their downstream effectors ROCK1 and ROCK2, were inhibited by treatment with Tat-C3, a cell-permeable Rho GTPase inhibitor (Sauzeau et al., 2001; Sekine et al., 1989), and Y-27632 and H-1152, two structurally distinct inhibitors of ROCK proteins (Uehata et al., 1997). Inhibition of either Rho or ROCK suppressed cell engulfment in suspended cultures (Figure 2A). Similar to LatB-treated cells, Rho- and ROCK-inhibited cells were able to aggregate but rarely internalized (Figures 2A and 2B and Movies S2A and S2B). These data implicate the Rho-ROCK-actin/myosin pathway as an important regulator of engulfment in suspension.

To determine whether cell internalization requires specific ROCK isoforms, ROCK1 and 2 expression were downregulated with short-interfering RNAs (siRNAs) (Figure 2Ca). Downregulation of either ROCK1 or ROCK2

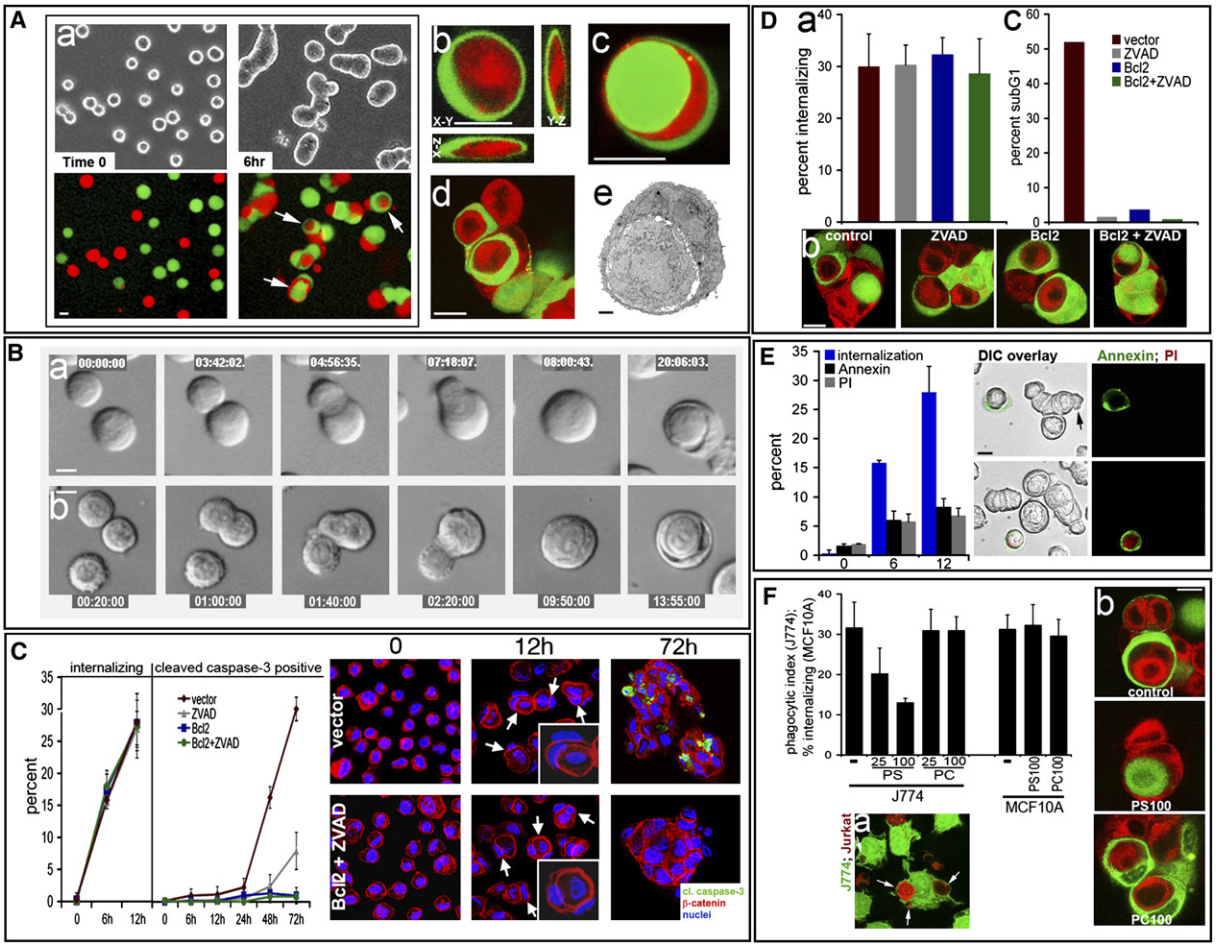

Figure 1. Suspended MCF10A Cells Internalize into Their Neighbors

(A) Microscopic examination of engulfment. (a) Phase contrast (top panels) and CellTracker fluorescent (bottom panels) images of suspended cells at 0 and 6 hr. Arrows mark engulfed cells. (b) Three-dimensional (3D) reconstruction of confocal Z series at 12 hr demonstrating complete internalization. Three-dimensional axes are labeled. (c and d) Confocal images of 12 hr CellTracker-labeled cells; scale bars are 10 μm. (e) Ultrastructure of 6 hr internalized cell; scale bar is 2 μm.

(B) DIC images from time-lapse of suspension cells. Times are hours:minutes:seconds. Scale bars are 10 μm. (a) One cell internalizes into another. (b) Two cells internalize into a third cell.

(C) Quantification of internalizing cells (left side of graph) and caspase-3 activation (right side of graph) in cytospins from ZVAD-FMK (ZVAD)-treated, Bcl2-overexpressing, or control (vector) cells. Data are means ± standard deviation (SD). Confocal images of β-catenin and cleaved caspase-3 stains of vector and ZVAD-treated Bcl2 cells 0, 12, and 72 hr after detachment are shown right of the graph. Arrows indicate internalized cells. The scale bar is 10 μm.

(D) (a) Quantification of internalizing cells in 12 hr vector control, ZVAD-treated, or Bcl2-overexpressing cultures by analysis of CellTracker-labeled cells. Data are means ± SD. (b) Confocal images of CellTracker-labeled cells at 12 hr; scale bar is 10 μm. (c) ZVAD and Bcl2 inhibit DNA fragmentation induced by UV irradiation. Graph shows % sub-G1 of UV-treated monolayer cultures. Data are representative of two independent experiments.

(E) Engulfment is not associated with PS exposure. % Annexin, and PI positivity are graphed versus cell internalization (from Figure 1C) at 0, 6, and 12 hr. Twelve hour DIC images are shown with Annexin (green) and PI (red) fluorescence. Arrow indicates internalizing intermediate. Fluorescent images are shown to the far right. The scale bar is 10 μm. Data are means ± SD.

(F) PS-liposomes do not inhibit cell internalization. Left side of graph depicts mean phagocytic index for engulfment of apoptotic Jurkat cells by J774 macrophages in the absence (–) or presence of 25 μM (25) or 100 μM (100) phosphatidylserine (PS) or phosphatidylcholine (PC) liposomes. Right side of graph depicts % internalizing MCF10A cells after 12 hr in the absence (–) or presence of 100 μM PS (PS100) or PC (PC100). Data are means ± SD. (a) Confocal image of CellTracker Green-labeled J774 cells that engulfed apoptotic CellTracker Red-labeled Jurkat cells (indicated by arrows). The scale bar is 10 μm. (b) Confocal images of CellTracker-labeled MCF10A cells after 12 hr in suspension in the absence (control) or presence of 100 uM PS (PS100) or 100 μM PC (PC100). The scale bar is 10 μm.

alone had only a minimal effect on the morphology of cells in monolayer culture; however, downregulation of both isoforms together reduced cell spreading and significantly altered cell morphology similarly to Y-27632 treatment (Figure 2Ca and data not shown). Similarly, ROCK1 and ROCK2 downregulation had an additive effect on cell

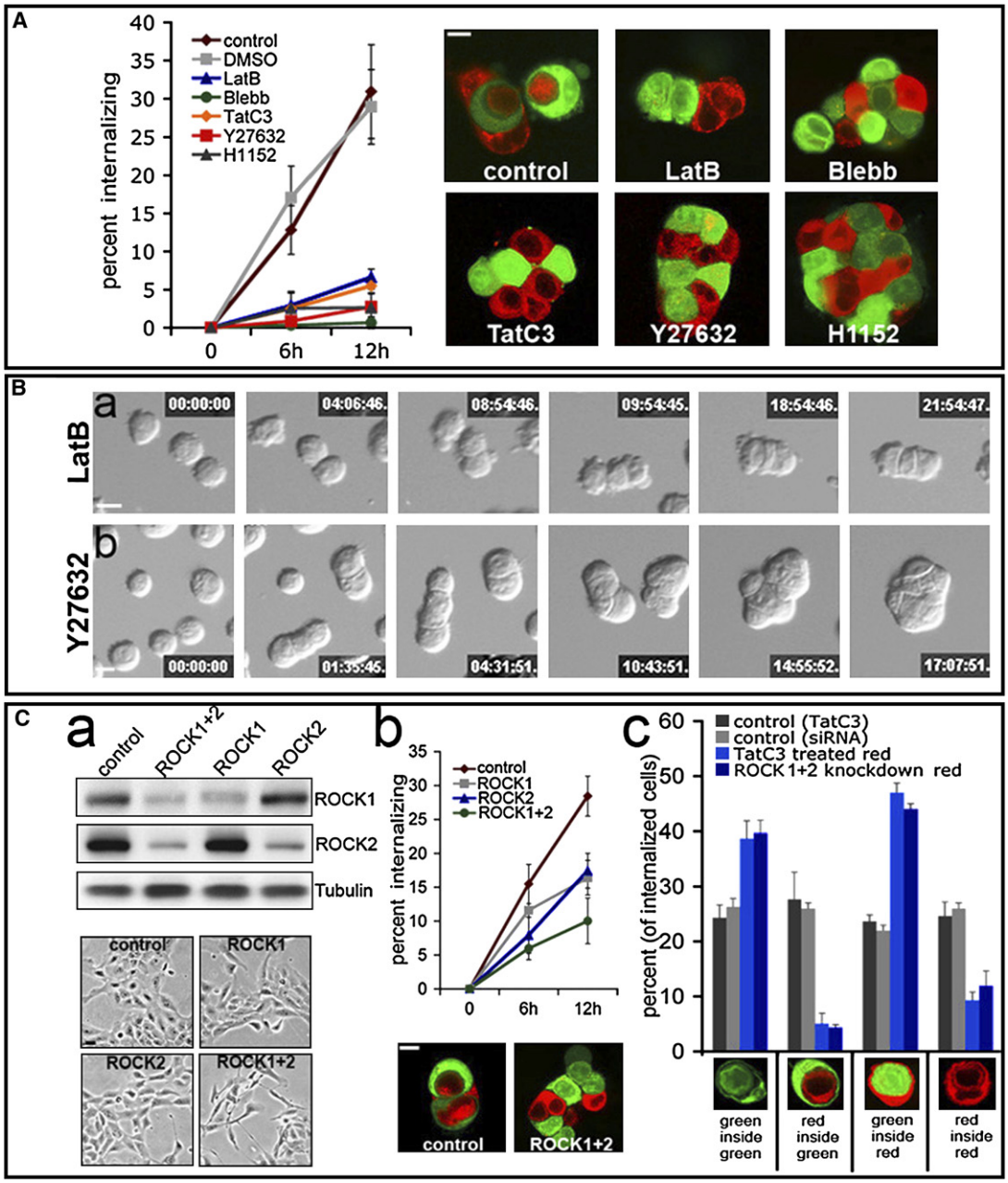

Figure 2. The Rho Pathway Is Required for Cell Internalization

(A) Inhibitors of engulfment. Graph depicts % internalizing cells for suspended MCF10A untreated (control) or treated with indicated inhibitors or DMSO at 6 and 12 hr. Confocal images of 12 hr CellTracker-labeled cells are shown to the right. The scale bar is 10 μm. Data are means ± SD.

(B) DIC images from time-lapse analysis of LatB (a) and Y-27632 (b) treated cells in suspension for approximately 20 hr. Times are hours:minutes: seconds. The scale bar is 10 μm.

(C) (a) Western blotting of control, ROCK1, or ROCK2 siRNA MCF10A lysates. Monolayer cultures are shown in the bottom images. The scale bar is 10 μm. (b) Internalization of control or ROCK1 and 2 siRNA transfected cells. Graph depicts % internalizing cells at 6 and 12 hr. Data are means ± SD. Confocal images of CellTracker-labeled cells are shown in the lower panels. The scale bar is 10 μm. (c) Rho and ROCK are required in internalizing cells. Percent of internalizing cells by color combination (CellTracker labels) is graphed at 6 hr of suspension. Green-labeled cells were untreated and mixed 1:1 with red-labeled cells treated with Tat-C3 or untreated (control) or transfected with ROCK1 and 2 siRNA or control siRNA. Examples of different color combinations of internalization are shown below the x axis. Data are means ± SD.

internalization, as the knockdown of both isoforms together inhibited internalization by approximately 3-fold compared to the less-than 2-fold effect of either isoform alone (Figure 2Cb).

Rho and ROCK Are Required in Internalizing Cells

To further probe the role of the Rho pathway we examined whether Rho or ROCK were required in internalizing cells or outer cells. CellTracker Red-labeled cells were pretreated with either Tat-C3 or ROCK1 and 2 siRNAs, mixed with untreated green-labeled control cells, and analyzed by confocal microscopy after 6 hr in suspension. Whereas engulfment was equally distributed between red- and green-labeled cells in control cultures, Rho- or ROCK-inhibited, red-labeled cells were rarely internalized into control green cells yet were able to function as outer cells to the same extent as controls (Figure 2Cc). Thus, the Rho pathway is specifically required in internalizing cells and not in outer cells. These data demonstrate that internalizing cells actively participate in this process in a Rho- and ROCK-dependent manner.

Given these unique features that distinguish this cell internalization process from phagocytic cell engulfment, we refer to this cell internalization process as entosis, after the Greek word entos, which means inside, into, or within.

MCF7 Cells Undergo Entosis

To determine if cells other than MCF10A undergo entosis, a panel of human cell lines was tested in suspension culture (Table S1). Cell engulfment was observed in a variety of nontumorigenic cell lines of various types and in four of nine tumor cell lines examined (Table S1). Among the tumor cell lines, MCF7 displayed the highest percentage (30%), and like MCF10A, internalization of these cells was dependent on ROCK and myosin II, and Rho was specifically required in internalizing cells and not in outer cells (Figure S4).

Cadherins Are Required for Entosis

Because epithelial cells form adherens junctions when cultured in suspension (Adams et al., 1998; Wrobel et al., 2004), and cells in our time-lapse analysis appeared to establish cell-cell junctions prior to internalizing (Figure 1B and Movies S1B and S1C), we examined whether cadherin-mediated adhesion is required for entosis. Cadherin proteins require calcium for binding activity and thus junctions can be blocked by chelating calcium from culture medium. The addition of either EGTA (chelates Ca^{2+}) or EDTA (chelates Ca^{2+} and Mg^{2+}) to suspension cultures strongly inhibited both aggregate formation and cell internalization of MCF7 and MCF10A cells (Figures 3Aa–3Ac), demonstrating a requirement for calcium-dependent processes.

To examine a requirement for cadherins more directly, cadherin-blocking antibodies were added to suspension cultures. Entosis of MCF7 cells was inhibited by the addition of an E-cadherin blocking antibody to almost the same extent as chelating calcium (Figure 3Aa), and like calcium chelation, blocking E-cadherin decreased cell aggregation (Figure S5). For MCF10A cells, which unlike MCF7 express high levels of both E- and P-cadherin (Figure S6), blocking E-cadherin alone had no effect, but a combination of E- and P-cadherin blocking antibodies inhibited cell internalization by approximately 2-fold (Figure 3Ab). These data demonstrate a requirement for adherens junctions to initiate entosis in suspension cultures.

Adherens Junctions Track Internalization

Suspension cultures were immunostained for E-cadherin and β-catenin to visualize cell junctions during entosis. By 6 hr after matrix detachment, many interacting cells displayed characteristic adherens junctions, with increased staining of E-cadherin and β-catenin at cell interfaces and dense plaques of these proteins at the points of maximum width between cells (Figure 3Ba), similar to what is described for epithelial cells undergoing compaction in a monolayer (Adams et al., 1998). For cells that were undergoing entosis, the extent of internalization was also tracked by increased intensity of E-cadherin and β-catenin staining and plaques at the terminal-most points of interaction between the inner and outer cells (Figures 3Bb–3Bd). These staining patterns suggest that the mechanism of entosis is directly linked to cell-cell compaction. TEM analysis showed that the closest contact between paired cells of engulfment intermediates was at the extreme end of finger-like projections of the receiving cell (Figure 3Ca), and many such sites contained characteristic adherens junctions (Figures 3Ca and 3Cb). Additionally, some projections of a receiving cell were interlocked with the inner cell (Figures 3Cb and 3Cc).

Entosis Results in Lysosomal Cell Death

To explore the fate of entotic cells we examined whether internalized cells would target to lysosomal compartments. Cells from suspension cultures were stained for three lysosome markers: LAMP1, an integral protein of the lysosome membrane; LysoTracker Red, which marks acidified compartments; and a fluorescent substrate of cathepsin B, a lysosomal protease. After 24 hr, approximately 10% of MCF7 cells were marked by prominent cathepsin B substrate or LysoTracker staining (Figure 4A). Immunostaining for LAMP1 together with β-catenin clearly demonstrated that lysosome-enveloped cells were internalized within another cell (Figure 4A). Similar staining patterns were also found for LAMP2 and LAMP3 (data not shown). The inhibition of ROCK by treatment with Y-27632 reduced the percentages of MCF7 nuclei that were marked with cathepsin B or LysoTracker Red staining or encircled by LAMP1 by ~10-fold, which correlates their occurrence with entosis (Figure 4A). To address whether internalized cells undergo cell death, suspended MCF7 cells were analyzed for DNA fragmentation by TUNEL, which labels DNA fragments generated during apoptosis or necrosis (Grasl-Kraupp et al., 1995) or during lysosomal digestion (McIlroy et al., 2000). Approximately 7% of cells were internalized and TUNEL positive, and

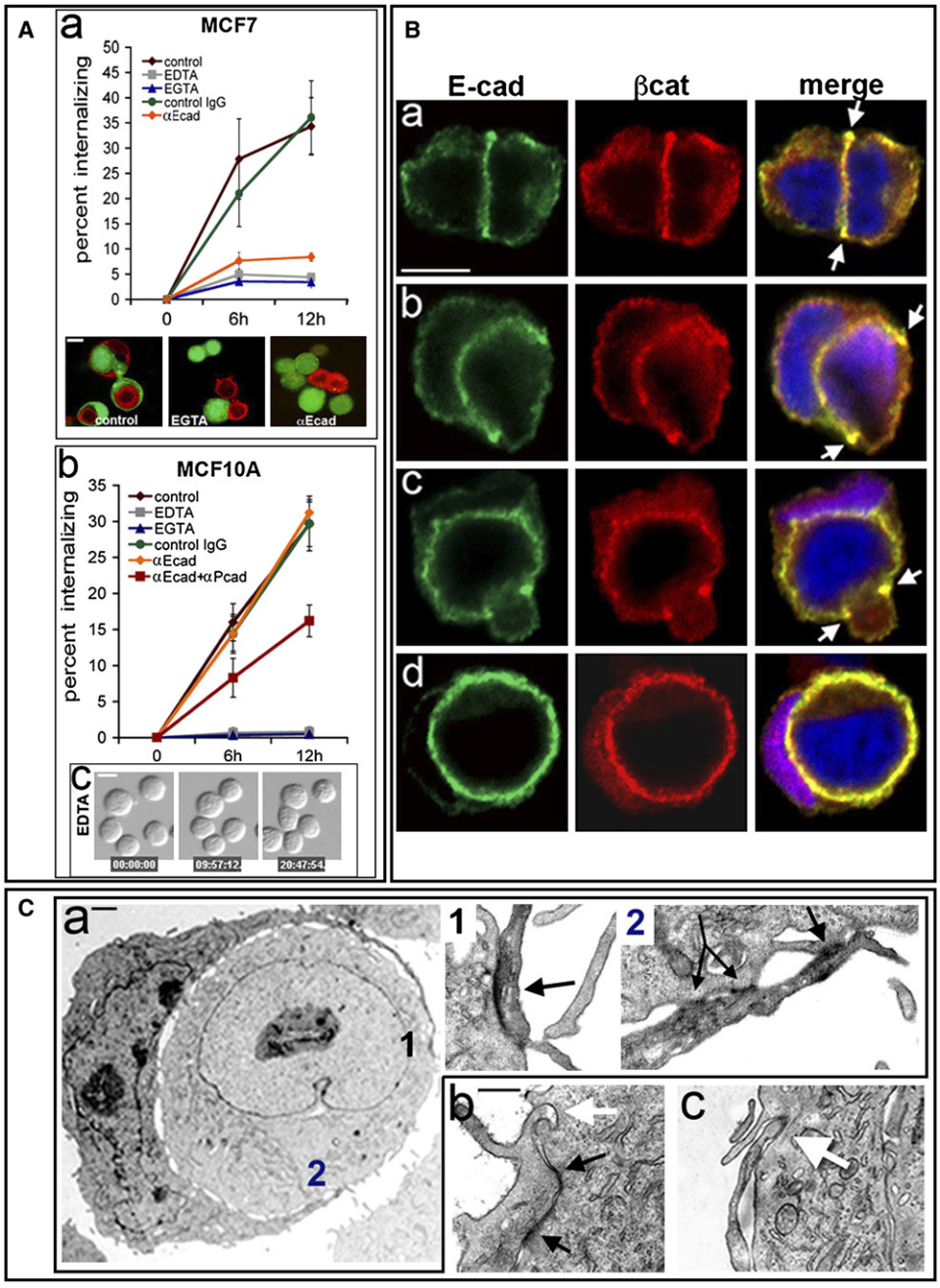

Figure 3. Adherens Junctions Are Required for Entosis

(A) Blocking cadherin function inhibits entosis. (a) Percent of internalizing cells in the presence of calcium chelators EDTA and EGTA, or E-cadherin (αE-cad) and P-cadherin (αP-cad) blocking, or control (control IgG) antibodies in suspended MCF7 cultures (a) or MCF10A cultures (b) at 6 and 12 hr. Data are means ± SD. Confocal images of CellTracker-labeled MCF7 cells are shown below the graph in (a). The scale bar is 10 μm. (c) DIC images from time-lapse of suspended MCF10A cells treated with EDTA. Times are hours:minutes:seconds. The scale bar is 10 μm.

(B) E-cadherin (green) (left panels) and β-catenin (red) (middle panels) staining of internalizing MCF10A cells. Right panels: overlayed images with nuclei (TO-PRO-3) (blue). The scale bar is 10 μm. (a) Suspended cells with adherens junction; plaques are marked by arrows. (b–d) Internalizing cells; plaques are marked by arrows.

(C) Ultrastructure of MCF10A internalizing cells. (a) Left panel shows internalizing intermediate. The scale bar is 2 μm. 1 and 2 indicate higher magnification shown in right panels. Arrows indicate adherens junctions. (b and c) Entosis intermediates showing interaction between inner and outer cells. Black arrows indicate adherens junctions; white arrows indicate interlocked outer and inner cells. The scale bar is 500 nm.

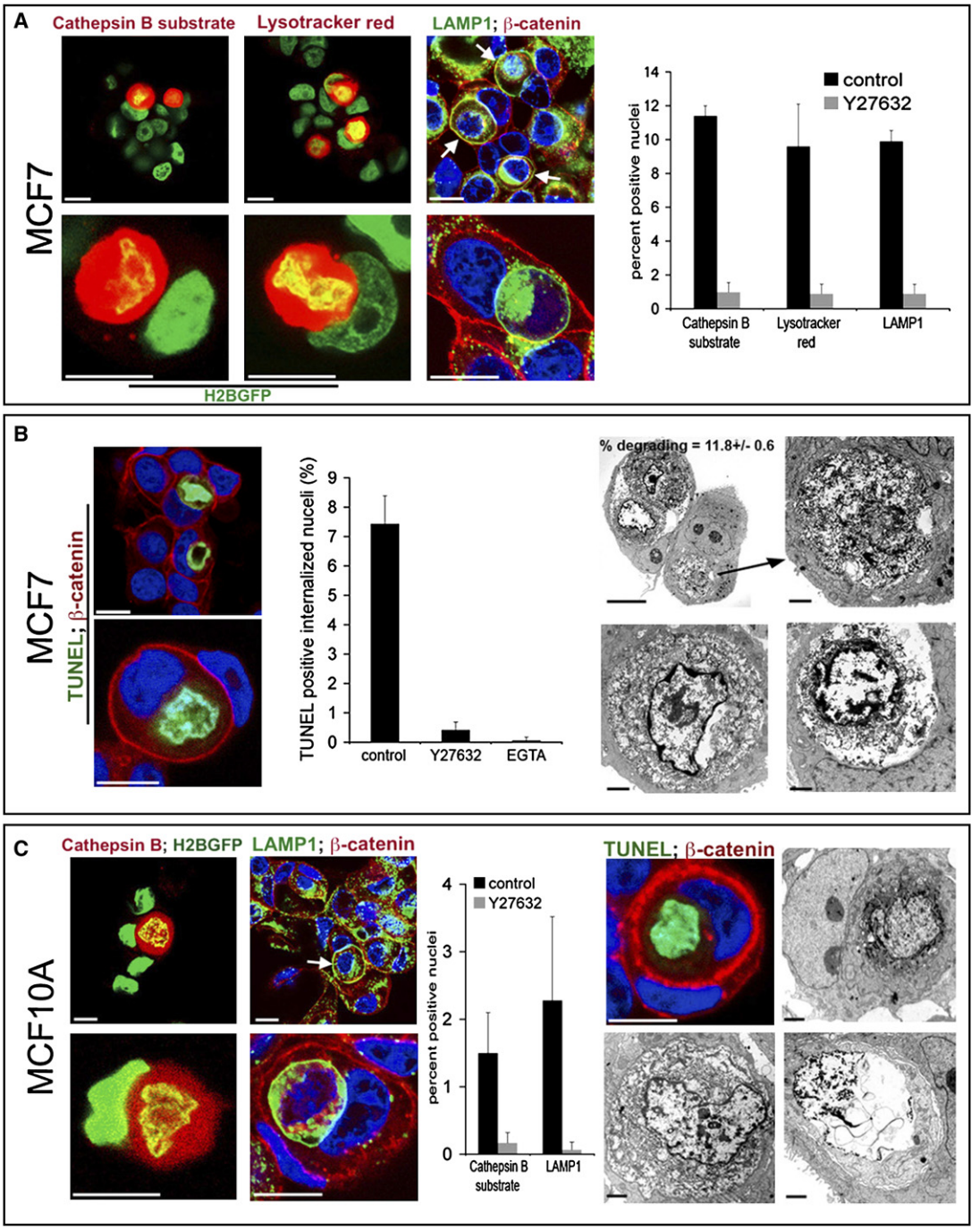

Figure 4. Internalized Cells Undergo Lysosome-Mediated Cell Death

(A) MCF7 cells in suspension stained for lysosome markers. Confocal images of H2B-GFP-expressing cells stained with cathepsin B substrate (left panels) or LysoTracker Red (middle panels) after 24 hr of suspension. Right panels: confocal images of immunofluorescent stains for LAMP1 (green), β-catenin (red), and nuclei (TO-PRO-3) (blue) on cytospin preparations at 24 hr of suspension. Arrows indicate LAMP1-encircled nuclei. The scale bars are 10 μm. Graph depicts % nuclei encircled by lysosome markers in control or Y-27632-treated cultures. Data are means ± SD.

(B) DNA fragmentation of internalized MCF7 cells. Left panels show cytospins stained for TUNEL (green), β-catenin (red), and nuclei (TO-PRO-3) (blue) after 48 hr of suspension. The scale bars are 10 μm. Graph shows % TUNEL-positive and internalized nuclei at 48 hr in control, Y-27632-, or EGTA-treated cultures. Data are means ± SD. Right panels: ultrastructure of internalized MCF7 cells at 24 hr suspension that are degrading. Arrow shows right top panel is enlarged area of left top panel. On the top left panel, % degrading cells is shown as mean ± SD of 200 cells in three serial sections spaced 50 μm. Scale bars are 10 μm in upper left panel, 2 μm in right and bottom panels.

this subset was inhibited by Y-27632 or the calcium chelator EGTA, correlating DNA fragmentation with entosis (Figure 4B). Finally, by TEM, 12% of suspended MCF7 cells displayed massive cellular and nuclear degradation that was devoid of apoptotic features, and all of these cells were internalized (Figure 4B).

MCF10A cells in suspension were also stained for cathepsin B activity and LAMP1 immunofluorescence. After 24 hr, 1%–2% of cells were marked by prominent cathepsin B substrate staining or encircled by LAMP1 in a ROCK-dependent manner (Figure 4C). This percentage of lysosome-targeted cells persisted but did not increase at 48 and 72 hr (data not shown). A similar percentage of internalized MCF10A cells were TUNEL positive and showed features of degradation by ultrastructure (Figure 4C and data not shown). Taken together, these data demonstrate that entosis in both MCF7 and MCF10A cells leads to lysosomal cell death.

Internalized Cells Can Be Released

To examine the fate of entotic cells in more detail, we followed internalized H2B-GFP-labeled MCF10A and MCF7 cells by time-lapse microscopy of cultures plated on untreated glass coverslips, which exhibit some entosis due to poor adherence. For both MCF10A and MCF7, the most common fate for internalized cells was death (70% for MCF7 and 49% for MCF10A), as evidenced by nuclear degradation and the eventual disappearance of some cells within the enveloping cell (Figure 5A and see Movie S4A). Surprisingly, 18% of internalized MCF10A cells and 12% of MCF7 were released from the outer cell back into the culture (Figure 5A and Movie S4B). These cells had a normal nuclear morphology and some underwent cell division subsequent to their release. The release of internalized cells was not unique to coverslip cultures as this was also observed with suspended cells (data not shown). Even more surprising is that a small percentage of cells (9% for MCF7 and 0.8% for MCF10A) underwent cell division while still internalized (Figure 5A and Movie S4C). These data support the conclusion that entotic cells are viable when they internalize. The remaining 32% of internalized MCF10A and 9% of MCF7 cells did not undergo any observable change over the 20 hr time course (Figure 5A).

Internalized Cells Can Die by Alternative Mechanisms

To examine the role of lysosome function in cell death, internalized cells were followed by time-lapse in the presence of concanamycin A (ConA) (Figure S7), an inhibitor of the vacuolar H^+/ATPase. ConA treatment did not dramatically alter the percentage of internalized cells that underwent cell death (37% versus 46% of control cells) but rather changed the nuclear morphology of dying cells from nonapoptotic to apoptotic (Figure 5Ba). Treatment of cells with the ionophore monensin (50 μM) yielded similar results; however, this reagent was also generally more toxic to MCF10A cells (data not shown). The majority (85%) of control cells that underwent cell death displayed nuclear disintegration without fragmentation (Figure 5Ba). Similarly 89% ± 2.5% of TUNEL-positive, internalized cells were negative for cleaved caspase-3 staining (Figure 5Bb), and 86% ± 2.4 of TUNEL-positive, cleaved caspase-3-negative nuclei showed evidence of disintegration without fragmentation (Figure 5Bb). These data suggest that internalized cells predominantly die by a nonapoptotic mechanism that is linked to lysosome function. Analysis of LysoTracker-stained cells by time-lapse also demonstrated that acidification is coincident with nuclear degradation (Figure S8 and Movie S5). In contrast, 100% of ConA-treated cells that died underwent DNA fragmentation (Figures 5Ba and 5Bb and Movie S4D), and fragmented nuclei in these cultures were positive for cleaved caspase-3 (Figure 5Bb). Moreover, these apoptotic cells were not absorbed into the outer cell but rather were retained in a large vacuole, presumably due to lysosome dysfunction (Movie S4D).

To follow the fate of cells in which apoptosis was inhibited, we performed time-lapse analysis of MCF10A cells overexpressing Bcl2 in the absence or presence of ConA. Death of internalized MCF10A-Bcl2 cells was inhibited nearly 2-fold (26% compared to 46% for control MCF10A), and of the detectable cell death events, 98% occurred by disintegration in the absence of DNA fragmentation, suggesting that Bcl2 is a strong inhibitor of apoptotic cell death of internalized cells and a partial inhibitor of nonapoptotic cell death (Figures 5Ba and 5Bb). Strikingly, treatment of Bcl2-overexpressing cells with ConA reduced the level of cell death to less than 1%. This nearly complete inhibition of cell death was associated with an increase in the release of internalized cells from 14%–15% (for Bcl2 and MCF10A controls) to 38% (Figure 5Ba). Together, these data demonstrate that lysosomal degradation is the predominant mechanism for elimination of internalized cells; however, an alternate apoptotic program can compensate to execute cell death when lysosomal function is disrupted.

Human Metastatic Breast Tumors Show Evidence of Entosis

The internalized cells detected in suspended MCF10A and MCF7 cultures closely resemble commonly observed cytological features referred to as cell-in-cell or cell cannibalism in clinical cancer specimens. Interestingly, these

(C) MCF10A cells in suspension for 24 hr stained for lysosome markers. Left panels: confocal images of H2B-GFP-expressing cells stained with cathepsin B substrate (far left panels); immunofluorescent stains for LAMP1 (green), β-catenin (red), and nuclei (TO-PRO-3) (blue) (right panels). The scale bars are 10 μm. Graph depicts % nuclei encircled by lysosome markers in control or Y-27632-treated cultures. Data are means ± SD. Right panels: top left image is TUNEL (green), β-catenin (red), and nuclei (TO-PRO-3) (blue) stained cytospin at 24 hr. Top right and bottom panels: ultrastructure of internalized cells with evidence of degradation. Scale bars are 10 μm in upper left panel, 2 μm in right and bottom panels.

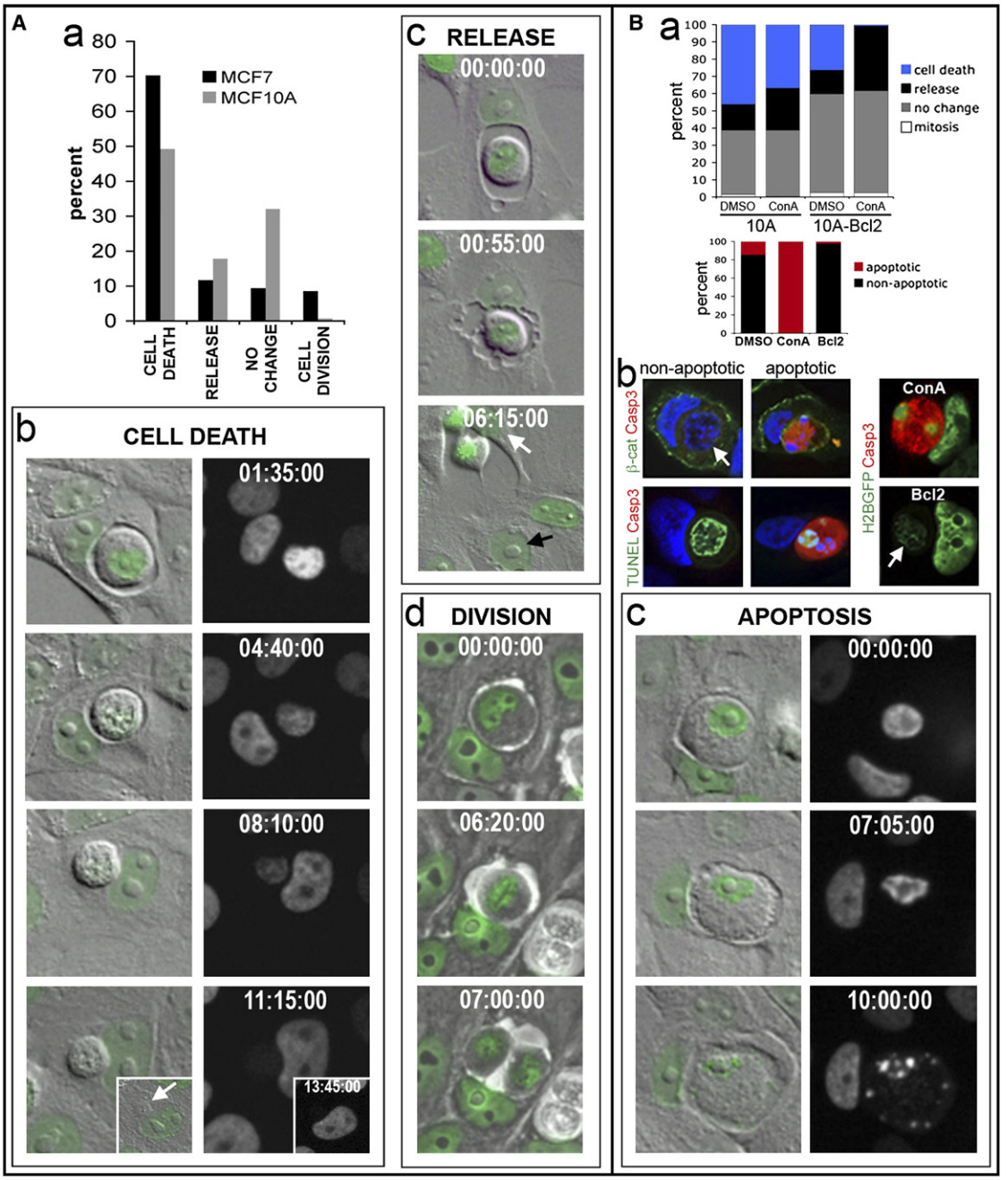

Figure 5. Time-Lapse Analysis of Internalized Cells

(A) (a) Quantification of cell fates for internalized cells. Percent of internalized MCF10A (n = 134) and MCF7 cells (n = 128) followed by time-lapse for approximately 20 hr is shown. (b–d) DIC (b and c) or phase contrast (d) and H2B-GFP fluorescence (green) (b–d) images of MCF10A cells. Times are hours:minutes:seconds. (b) Internalized cell undergoes cell death. Inset in lower panels: internalized cell disappears into outer cell; arrow marks inner cell. (c) Internalized cell is released. White arrow marks previously internalized cell; black arrow marks outer cell. (d) Internalized cell divides.

(B) Cell fates with lysosome and apoptosis inhibition. (a) Upper graph: quantification of cell fates for internalized ConA-treated MCF10A cells (n = 103) or DMSO control (n = 134) or ConA-treated MCF10A-Bcl2 cells (n = 125) or DMSO control (n = 152). Lower graph: quantification of cell death morphology in MCF10A cells treated with DMSO or ConA or DMSO-treated MCF10A-Bcl2 cells. Note nonapoptotic cells did not exhibit nuclear fragmentation. (b) Confocal images of nonapoptotic or apoptotic cell death are shown below the graphs. Left panels: nonapoptotic death of internalized MCF10A cells stained for cleaved caspase-3 and β-cat (upper image) or TUNEL (lower image). Middle panels: apoptotic death of internalized MCF10A cells stained for cleaved caspase-3 and β-cat (upper image) or TUNEL (lower image). Nuclei were stained with DAPI. Right panels: cells from time-lapse (expressing H2B-GFP [green]) stained for cleaved caspase-3 (red). Upper image: MCF10A cell treated with ConA. Lower image: MCF10A-Bcl2 cell treated with DMSO. Arrow marks degrading nucleus that is negative for cleaved caspase-3. (c) Internalized ConA-treated MCF10A cell undergoes apoptosis. Panels show DIC and H2B-GFP fluorescence (green) images from time-lapse. Times are hours:minutes:seconds.

features are most frequently detected in metastatic tumor cells that grow in a partial state of suspension in fluid exudates, for example in the pleural space surrounding the lungs (Gupta and Dey, 2003). To investigate the nature of cell-in-cell structures in human metastatic tumors, we immunostained breast tumor cells harvested from the pleural fluid of patients. Cells were stained with antibodies directed against β-catenin and MUC-1 to label the tumor cell population. Seven of eight exudate samples that were analyzed displayed some tumor cell internalization with most showing 1% to 2%, and one (#2) displayed a high level (20%) of cell-in-cell tumor structures (Figure 6A). The majority of internalized cells in this sample were negative for cleaved caspase-3 (96% negative), and nearly 40% were encircled by LAMP1 staining (Figure 6C). Cell-in-cell intermediates displayed increased intensity of β-catenin at cell-cell interfaces, and some also displayed plaques at the most distant points of contact between the inner and outer cells (Figure 6C, arrows). Effusion sample #4 had a sufficient quantity of tumor cells to analyze cell-in-cell by ultrastructure. By TEM, we could find fully internalized cells that appeared to be viable (i.e., no evidence of apoptosis or necrosis), as well as intermediates that resembled the in vitro structures, with close contact between two cells at the end of finger-like projections where we observed adherens junctions (Figures 6D and S9). Thus, the cell-in-cell structures associated with human tumor cells display similar morphological features as the suspended MCF10A and MCF7 cells. Therefore, entosis in suspension cultures in vitro mimics distinguishing features of the cell-in-cell phenomenon in human tumor cells in fluid exudates.

Human Primary Breast Tumors Show Evidence of Entosis

Recently the cell-in-cell cytological feature was described in primary breast tumors in addition to metastatic tumor exudates (Abodief et al., 2006). We investigated a panel of 20 primary human breast carcinomas by H&E or immunohistochemical staining and found that 11 of these displayed features consistent with cell-in-cell (data not shown). Sections from four tumors with the highest number of these structures were immunostained for β-catenin and cleaved caspase-3 or fragmented DNA (TUNEL). All four tumors exhibited evidence of live-cell internalization consistent with entosis, at a frequency of ~0.5%–2.5% of the total tumor cell population (Figure 6E). Many internalized cells had a normal nuclear morphology and a majority, ~75%–90%, were negative for cleaved caspase-3 staining (Figure 6E). We also detected structures containing a cell within a cell that was inside of another cell, as observed in suspended cultures (Figure 6E, first two panels). These data demonstrate that cells with a normal nuclear morphology and negative for either cleaved caspase-3 or TUNEL staining are internalized by adjacent tumor cells in primary human breast tumors, which is consistent with entosis.

To characterize a wider variety of human solid tumors for entosis, tumor tissue arrays with sections representing multiple tumor types were stained for β-catenin alone or with cytokeratin 5, a basal epithelial marker, and samples were analyzed for engulfment by microscopy. Similar to the breast tumors, we observed cell internalization in a wide variety of these tumor samples (Figure 6G), typically in 0.3%–2% of the total tumor cell population in positive samples. We conclude that entosis is a feature commonly observed in both metastatic and primary human tumors of many types.

DISCUSSION

In this report, we describe a cell death mechanism that is provoked by loss of attachment to ECM and occurs independent of apoptotic processes previously shown to be associated with death of matrix-deprived cells (Gilmore, 2005). While this cell death process and apoptosis both can result in the internalization of one cell inside of another, the mechanisms responsible for cell internalization are highly distinguishable. Unlike the phagocytic ingestion of apoptotic cells, cell internalization in suspension is not associated with caspase activation nor driven by phosphatidylserine exposure (Fadok et al., 1992) but rather is dependent on adherens junctions and is driven by Rho and ROCK activity in internalizing cells, which is consistent with a cell invasion rather than an engulfment process. Moreover, internalized cells can be released or undergo cell division, which highlights a further distinguishing aspect between these two processes—unlike dying cells that are cleared by phagocytosis, internalized cells in suspension are alive. Taken together, these distinguishing features prompted us to assign this process the name entosis, after the Greek word entos, which means inside, into, or within.

While the detailed mechanisms mediating entosis remain to be elucidated, the data presented here provoke consideration of a model to explain how a Rho-dependent process involving actin polymerization and myosin II activity can mediate cell internalization. Figure 7 presents the simplest working model for entosis based on our experimental findings. We propose that unbalanced myosin II-dependent force associated with adherens junction compaction drives one cell to push into another (Figure 7). During adherens junction formation between attached cells, compaction is associated with translocation of the cell body toward the maturing junction by the myosin clutch mechanism, in which myosin II-driven retrograde flow pulls against actin cables that are anchored by cadherins, producing contractile force that translocates the cell body (Adams and Nelson, 1998). Previously it has been shown that force generated by actomyosin contraction downstream of integrin engagement can directly oppose cell-cell adhesion force (de Rooij et al., 2005; Ryan et al., 2001). We found that the addition of reconstituted basement membrane (Matrigel) to suspended cultures inhibited cell internalization in a β1-integrin-dependent manner (Figure S10). Thus it is possible that integrin engagement acts as a counterbalancing force that

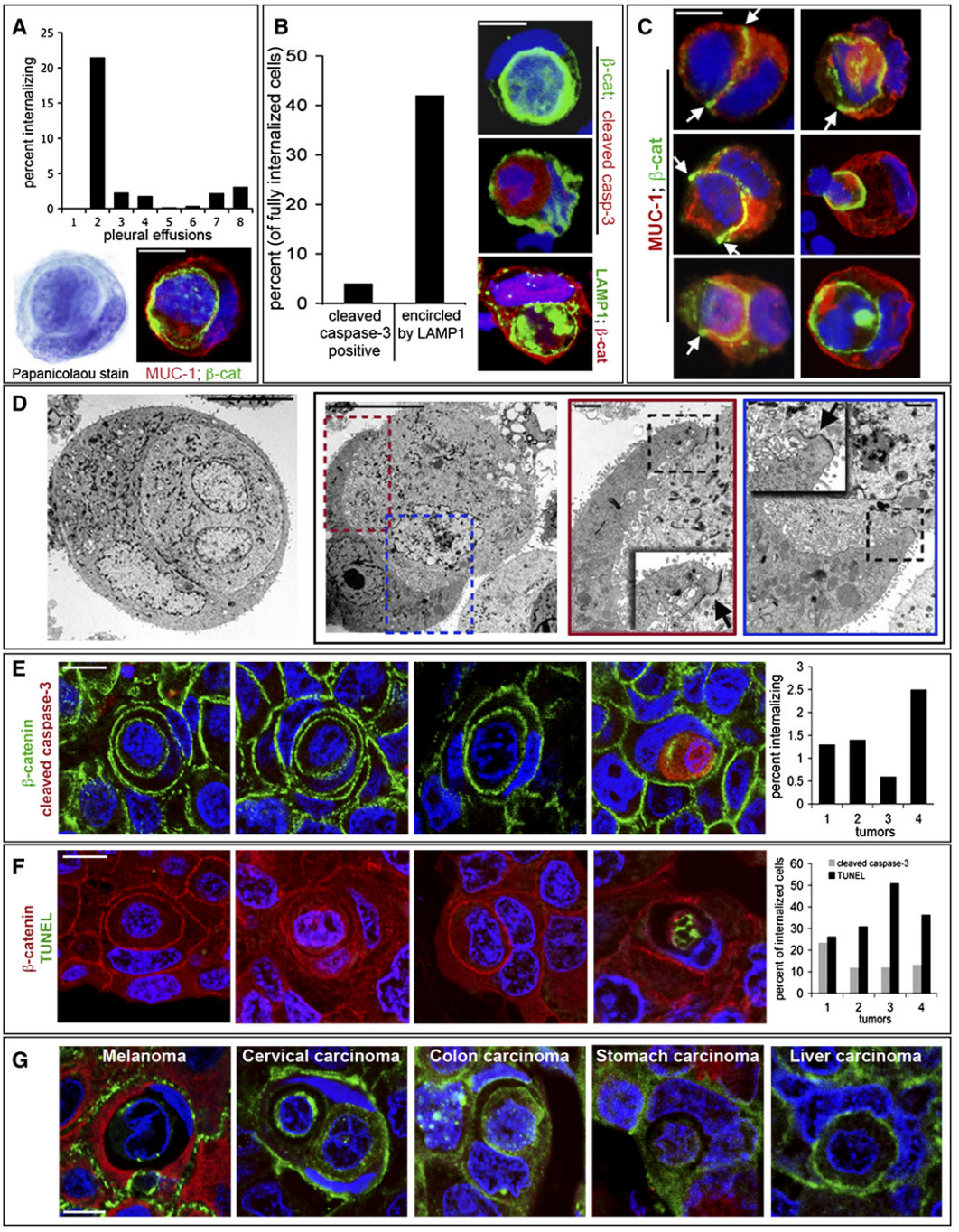

Figure 6. Entosis in Human Tumors

(A) Quantification of internalizing cells in fluid exudates from metastatic breast carcinomas cytospun directly from pleural fluid. Graph shows % internalizing of 200 tumor cells assayed by microscopic analysis of MUC-1 and β-cat immunofluorescent stains. Bottom left panel: Papanicolaou stain of internalized cell from pleural effusion 2. Bottom right panel: confocal image of internalized tumor cell stained for MUC-1 (red), β-cat (green), and nuclei (TO-PRO-3) (blue) from pleural effusion 2. The scale bar is 10 μm.

(B) Cleaved caspase-3 and LAMP1 staining of entosis from pleural effusion #2. Graph depicts % of fully internalized cells that were positive for cleaved caspase-3 (n = 100) or encircled by LAMP1 staining (n = 30) ("inside lysosome"). Top and middle panels are immunofluorescent stains for β-cat (green), cleaved caspase-3 (red), and nuclei (TO-PRO-3) (blue). Top panel: internalized cell is negative for cleaved caspase-3. Middle panel: internalized cell is positive for cleaved caspase-3. Bottom panel: internalized cell stained for β-cat (red) and LAMP1 (green); note internalized cell is encircled by ring of LAMP1 staining. The scale bar is 10 μm.

(C) MUC-1 and β-catenin stains of entosis intermediates from pleural effusions. Top panels show images from effusions #4 (left image) and #8 (right image). Left image shows adherens junction between paired tumor cells; right image shows internalizing intermediate; arrows mark β-cat plaques.

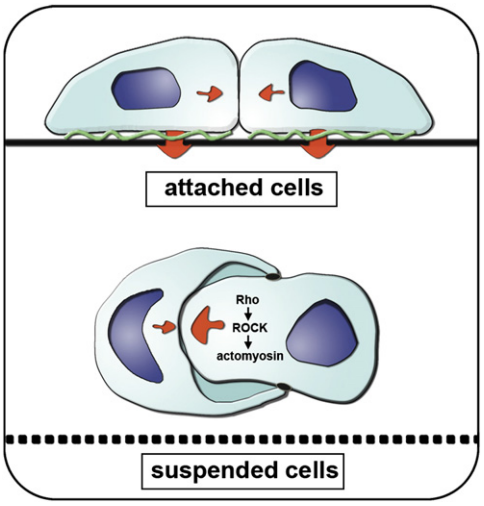

Figure 7. Model for Entosis in Matrix-Deprived Cells

Top panel: The force of adherens junction compaction (small red arrows) is normally balanced by matrix attachment (large red arrows). Bottom panel: In the absence of integrin engagement, differences in Rho- and myosin II-dependent cell compaction force (red arrows) can drive one cell to invade or push into another.

prevents entosis during cell-cell compaction of adherent cells. When cells that are detached from matrix interact and undergo compaction, we propose that an imbalance in contractile force between two cells could result in one cell pushing into, and thus being wrapped around by, the other.

We also note similarities between entosis and the invasion of mammalian cells by a particular class of parasites, Apicomplexa, which use an adhesion-based motility system involving a moving junction and an actomyosin-based "glideosome" to invade host cells (Opitz and Soldati, 2002). Invasion is an active process that is mediated by the parasite's cytoskeleton, and the host cell does not appear to play an active role in uptake. By ultrastructure, the attachment points between inner and outer cells during entosis (Figure 3C) are strikingly similar to the attachments between Apicomplexa parasites and mammalian cells during invasion (Aikawa et al., 1978). Also, in some time-lapse videos of MCF7 cells undergoing entosis in soft agar (see below), an attachment point between inner and outer cells indeed appears to move as a ring along the internalizing cell body, similar to the first descriptions of moving junctions in Apicomplexa (Figure S11 and Movie S6) (Aikawa et al., 1978). Thus, it is plausible that internalizing entotic cells ratchet a moveable junction similar to Apicomplexa parasites. Finally, we note that while the data presented here are consistent with the invasion of one cell into another, they do not completely rule out other scenarios, such as a more active role for outer cells or a role for the Rho pathway in mediating a shape or adhesive change in internalizing cells.

Our data demonstrate that entosis is one mechanism that underlies the formation of cell-in-cell structures that have been widely reported in human tumors for over 25 years, including breast carcinoma (Abodief et al., 2006; Uei et al., 1980), lung carcinomas (Craig et al., 1983; DeSimone et al., 1980), endometrial stromal carcinoma (Hong, 1981), and many others that are too numerous to list here. Elucidation of the mechanism underlying these long-standing observations in human tumors should lay the groundwork for investigating the consequences of cell-in-cell or entosis on human tumor initiation and progression. It should be noted that we cannot rule out with certainty that this process could occur in samples ex vivo as a stress response associated with tumor removal.

Several possibilities are feasible for how entosis, or live cell-in-cell invasion, could affect tumor growth. For example, entosis could provide nutrients for the survival of tumor cells lacking appropriate vascular access. We have found that cells in suspension are metabolically impaired (J. Debnath, Y. Irie, Z. Schafer, S. Gao, and J.S.B., unpublished data). However, we were unable to detect any correlation between entosis and autophagy in MCF10A or MCF7 cells expressing LC3-GFP, a fluorescent label of autophagic vacuoles. Moreover, entosis was reduced in the absence of serum (data not shown), as was reported for a similar process in cultured lung tumor cells (Brouwer et al., 1984), suggesting that entosis is unlikely to function as a starvation response mechanism to generate increased metabolic substrate.

It is also possible that entosis could promote tumorigenesis by facilitating cell fusion and the development of aneuploidy, as was suggested for a similar engulfment

Middle panels show entosis intermediates from effusions #8 (left image) and #2 (right image); arrows mark β-cat plaques. Bottom left panel: entosis intermediate from effusion #7; arrow marks β-cat plaque. Bottom right panel: fully internalized cell from effusion #2; note intense β-cat staining surrounding internalized cell. The scale bar is 10 μm.

(D) Ultrastructural analysis of internalizing tumor cells from pleural effusion #3. Left panel: fully internalized cell. Right panels: internalizing intermediate. Red and blue hatched boxes demarcate areas for red- and blue-labeled right panels. Black hatched boxes mark insets; arrows mark adherens junctions.

(E) Human breast tumors stained for β-cat (green), cleaved caspase-3 (red), and nuclei (TO-PRO-3) (blue). Left three panels: internalized cells are negative for cleaved caspase-3 staining. Far right panel: internalized cell is cleaved caspase-3 positive. Graph shows % internalized cells of 500 tumor cells assessed by β-cat staining for four primary human breast carcinomas.

(F) Human breast tumors stained for β-cat (red), TUNEL (green), and nuclei (TO-PRO-3) (blue). Left three panels: internalized cells are negative for TUNEL staining. Far right panel: internalized cell is TUNEL positive. Graph shows % of internalized cells positive for cleaved caspase-3 staining (gray bars) out of 50 or TUNEL staining (black bars) out of 30 internalized cells.

(G) Representative images of internalized cells in human solid tumors. Melanoma and stomach carcinoma panels: staining for β-cat (green), cytokeratin 5 (red), and nuclei (TO-PRO-3) (blue) staining. All other panels were stained for β-cat (green) and nuclei (TO-PRO-3) (blue).

process in HEK293 cells induced by expression of myristoylated Akt2 (Jin and Woodgett, 2005). It is interesting to note that HEK293 cells in this report were also partially detached as a result of Akt2 activation, raising the possibility that these cells were undergoing a similar process to what we describe here, as a secondary consequence of detachment. In our experiments with MCF10A and MCF7 cells, we were unable to detect cell fusion in any internalized cells followed by time-lapse microscopy. We also examined cell fusion in suspension cultures by mixing populations with different selectable markers and double-selecting for fusion clones. While we were able to detect some cell fusion events by this method (~0.01%), these were not inhibited by Y-27632, a potent inhibitor of entosis (Figure S12). Thus, to date we have no evidence that cells can fuse as a result of entosis.

Finally, entosis could function as an intrinsic tumor suppression mechanism to eliminate cells that are outside their natural niches. The presence of a tumor-suppressive cell engulfment process was previously postulated based on observations of a similar process in lung tumor cells (Brouwer et al., 1984). Within the solid tumors exhibiting entosis in this study, we were unable to detect deposition of the matrix proteins laminin, collagen IV, or fibronectin in regions of tumor cells away from the basement membrane (Figure S13), suggesting that loss of matrix attachment could provoke this process in human tumors as it does in cultured cells. To model the potential for entosis to limit tumor growth, we assayed MCF7 cells in anchorage-independent growth assays in soft agar. We noted the presence of cell-in-cell, or entotic structures in soft agar that were inhibited by Y-27632 treatment (Figures S14A and S7). Y-27632 treatment also increased colony formation by ~10-fold, and continual treatment increased colony size by ~1.5-fold (Figure S14C). In analysis of soft agar cultures by time-lapse, we discovered that, following mitosis, daughter cells internalize into each other (Figure S14A and Movie S7). Of 12 single cells that were followed by time-lapse for ~60 hr from the start of soft agar growth, 8 underwent cell division followed by the internalization of one daughter cell into the other. This demonstrates that entosis could oppose proliferation to inhibit the number and size of soft agar colonies. While we cannot rule out the possibility that ROCK inhibits colony formation by another mechanism, these data raise the possibility that entosis could suppress tumor growth.

In summary, we have identified a nonapoptotic cell death mechanism, entosis, that occurs in cell populations deprived of matrix attachment. These data present a context and model with which to define the cell-in-cell or cannibalism cytological feature of human tumors. Moreover, the data presented here suggest that a fundamental epithelial cell process, the formation of adherens junctions, can be directly linked to a nonapoptotic cell death mechanism in the absence of a critical checkpoint, integrin engagement. While our data are consistent with a tumor-suppressive function, further studies are required to more precisely define the effect of entosis on tumor growth.

EXPERIMENTAL PROCEDURES

Cell Culture Antibodies and Reagents

All cell lines, antibodies, and reagents used in this study are supplied as Supplemental Data. Additional experimental details for each section are supplied as Supplemental Data.

Cell Internalization Assays

(1) Cytospin immunofluorescence assays. Single-cell suspensions were plated on polyhema-coated plates, cytospun onto glass slides at the indicated times, and analyzed by immunofluorescence.
(2) CellTracker assays. Monolayer cultures were stained with CellTracker Red or Green (Invitrogen), treated with the indicated inhibitors, trypsinized, and plated as in (1). At the indicated times, suspended cells were stained with Hoechst 33342 (5 μg/ml for 15 min at 37°C), embedded in 0.5% agar, and mounted onto glass slides.

LysoTracker and Cathepsin B Substrate Staining

LysoTracker Red or cathepsin B substrate was added to suspension cultures of H2B-GFP-expressing cells (Wang et al., 2007) for 10–30 min at 37°C. Cells were fixed, embedded in agar, and mounted as described for cell engulfment assays above.

Time-Lapse Microscopy

Time-lapse microscopy was performed as described (Shi and King, 2005). Cells were grown as monolayers on coverglass bottom dishes (MatTek, Ashland, MA) or in suspension on polyhema-coated dishes (Overholtzer et al., 2006). Images were obtained every 5, 10, or 12 min for the indicated time courses.

Human Tumors

Pleural effusions were centrifuged and washed in PBS. Red blood cells were lysed with Hybri-Max red blood cell lysis buffer (Sigma #R7757), and tumor cells were cytospun in a cytocentifuge 7620 (Wescor) and processed for immunofluorescence. Human primary breast tumor sections were deparraffinized in xylene and washed in ethanol. Sections were retrieved in Antigen Unmasking Solution (Vector #H-3300) for β-cat and TUNEL and in 10 mM EDTA for cleaved caspase-3 staining. Human tumor tissue arrays were purchased from US Biomax.

For Experimental Procedures sections describing immunofluorescent staining, western blotting, siRNA, surface biotinylation, phagocytosis assays and liposomes, TUNEL, Annexin staining, TEM, cell fusion assay, and growth in soft agar, see Supplemental Experimental Procedures.

Supplemental Data

Supplemental Data include Supplemental Experimental Procedures, fourteen figures, one table, and thirteen movies and can be found with this article online at http://www.cell.com/cgi/content/full/131/5/966/DC1/.

ACKNOWLEDGMENTS

We thank Andrea Richardson for first pointing out the cell-in-cell cytological features reported in the literature, Jayanta Debnath for the LC3-GFP construct and helpful discussions, Amy Hall and other members of the Brugge laboratory for helpful discussions, Jennifer Waters and Lara Petrak of the Nikon Imaging Center for microscopy, and Elizabeth Bennecchi and Maria Ericsson for TEM. The work was funded by grants CA080111 (J.S.B.) and CA089393 (J.S.B. and S.J.S.) from the National Cancer Institute as well as the Breast Cancer Research Foundation (J.S.B.), the National Cancer Institute/National Institutes of Health (NIH) Institutional Training Grant T32CA09361 (M.O.), NIH

GM66492 (R.W.K.), and The Susan G. Komen Breast Cancer Foundation (PDF29406) (A.A.M.).

Received: March 26, 2007
Revised: August 6, 2007
Accepted: October 23, 2007
Published: November 29, 2007

REFERENCES

Abodief, W.T., Dey, P., and Al-Hattab, O. (2006). Cell cannibalism in ductal carcinoma of breast. Cytopathology *17*, 304–305.

Adams, C.L., and Nelson, W.J. (1998). Cytomechanics of cadherin-mediated cell-cell adhesion. Curr. Opin. Cell Biol. *10*, 572–577.

Adams, C.L., Chen, Y.T., Smith, S.J., and Nelson, W.J. (1998). Mechanisms of epithelial cell-cell adhesion and cell compaction revealed by high-resolution tracking of E-cadherin-green fluorescent protein. J. Cell Biol. *142*, 1105–1119.

Aikawa, M., Miller, L.H., Johnson, J., and Rabbege, J. (1978). Erythrocyte entry by malarial parasites. A moving junction between erythrocyte and parasite. J. Cell Biol. *77*, 72–82.

Brouwer, M., de Ley, L., Feltkamp, C.A., Elema, J., and Jongsma, A.P. (1984). Serum-dependent "cannibalism" and autodestruction in cultures of human small cell carcinoma of the lung. Cancer Res. *44*, 2947–2951.

Chautan, M., Chazal, G., Cecconi, F., Gruss, P., and Golstein, P. (1999). Interdigital cell death can occur through a necrotic and caspase-independent pathway. Curr. Biol. *9*, 967–970.

Craig, I.D., Desrosiers, P., and Lefcoe, M.S. (1983). Giant-cell carcinoma of the lung. A cytologic study. Acta Cytol. *27*, 293–298.

de Rooij, J., Kerstens, A., Danuser, G., Schwartz, M.A., and Waterman-Storer, C.M. (2005). Integrin-dependent actomyosin contraction regulates epithelial cell scattering. J. Cell Biol. *171*, 153–164.

Debnath, J., Baehrecke, E.H., and Kroemer, G. (2005). Does autophagy contribute to cell death? Autophagy *1*, 66–74.

Debnath, J., Mills, K.R., Collins, N.L., Reginato, M.J., Muthuswamy, S.K., and Brugge, J.S. (2002). The role of apoptosis in creating and maintaining luminal space within normal and oncogene-expressing mammary acini. Cell *111*, 29–40.

Degterev, A., Huang, Z., Boyce, M., Li, Y., Jagtap, P., Mizushima, N., Cuny, G.D., Mitchison, T.J., Moskowitz, M.A., and Yuan, J. (2005). Chemical inhibitor of nonapoptotic cell death with therapeutic potential for ischemic brain injury. Nat. Chem. Biol. *1*, 112–119.

DeSimone, P.A., East, R., and Powell, R.D., Jr. (1980). Phagocytic tumor cell activity in oat cell carcinoma of the lung. Hum. Pathol. *11*, 535–539.

Fadok, V.A., Bratton, D.L., Rose, D.M., Pearson, A., Ezekewitz, R.A., and Henson, P.M. (2000). A receptor for phosphatidylserine-specific clearance of apoptotic cells. Nature *405*, 85–90.

Fadok, V.A., Voelker, D.R., Campbell, P.A., Cohen, J.J., Bratton, D.L., and Henson, P.M. (1992). Exposure of phosphatidylserine on the surface of apoptotic lymphocytes triggers specific recognition and removal by macrophages. J. Immunol. *148*, 2207–2216.

Frisch, S.M., and Francis, H. (1994). Disruption of epithelial cell-matrix interactions induces apoptosis. J. Cell Biol. *124*, 619–626.

Gilmore, A.P. (2005). Anoikis. Cell Death Differ. *12* (*Suppl 2*), 1473–1477.

Grasl-Kraupp, B., Ruttkay-Nedecky, B., Koudelka, H., Bukowska, K., Bursch, W., and Schulte-Hermann, R. (1995). In situ detection of fragmented DNA (TUNEL assay) fails to discriminate among apoptosis, necrosis, and autolytic cell death: a cautionary note. Hepatology *21*, 1465–1468.

Gupta, K., and Dey, P. (2003). Cell cannibalism: diagnostic marker of malignancy. Diagn. Cytopathol. *28*, 86–87.

Hong, I.S. (1981). The exfoliative cytology of endometrial stromal sarcoma in peritoneal fluid. Acta Cytol. *25*, 277–281.

Jacobson, M.D., Weil, M., and Raff, M.C. (1997). Programmed cell death in animal development. Cell *88*, 347–354.

Jin, J., and Woodgett, J.R. (2005). Chronic activation of protein kinase Bbeta/Akt2 leads to multinucleation and cell fusion in human epithelial kidney cells: events associated with tumorigenesis. Oncogene *24*, 5459–5470.

Lockshin, R.A., and Zakeri, Z. (2004). Caspase-independent cell death? Oncogene *23*, 2766–2773.

Mailleux, A.A., Overholtzer, M., Schmelzle, T., Bouillet, P., Strasser, A., and Brugge, J.S. (2007). BIM regulates apoptosis during mammary ductal morphogenesis, and its absence reveals alternative cell death mechanisms. Dev. Cell *12*, 221–234.

McIlroy, D., Tanaka, M., Sakahira, H., Fukuyama, H., Suzuki, M., Yamamura, K., Ohsawa, Y., Uchiyama, Y., and Nagata, S. (2000). An auxiliary mode of apoptotic DNA fragmentation provided by phagocytes. Genes Dev. *14*, 549–558.

Meredith, J.E., Jr., Fazeli, B., and Schwartz, M.A. (1993). The extracellular matrix as a cell survival factor. Mol. Biol. Cell *4*, 953–961.

Monks, J., Rosner, D., Geske, F.J., Lehman, L., Hanson, L., Neville, M.C., and Fadok, V.A. (2005). Epithelial cells as phagocytes: apoptotic epithelial cells are engulfed by mammary alveolar epithelial cells and repress inflammatory mediator release. Cell Death Differ. *12*, 107–114.

Opitz, C., and Soldati, D. (2002). 'The glideosome': a dynamic complex powering gliding motion and host cell invasion by Toxoplasma gondii. Mol. Microbiol. *45*, 597–604.

Overholtzer, M., Zhang, J., Smolen, G.A., Muir, B., Li, W., Sgroi, D.C., Deng, C.X., Brugge, J.S., and Haber, D.A. (2006). Transforming properties of YAP, a candidate oncogene on the chromosome 11q22 amplicon. Proc. Natl. Acad. Sci. USA *103*, 12405–12410.

Ryan, P.L., Foty, R.A., Kohn, J., and Steinberg, M.S. (2001). Tissue spreading on implantable substrates is a competitive outcome of cell-cell vs. cell-substratum adhesivity. Proc. Natl. Acad. Sci. USA *98*, 4323–4327.

Sauzeau, V., Le Mellionnec, E., Bertoglio, J., Scalbert, E., Pacaud, P., and Loirand, G. (2001). Human urotensin II-induced contraction and arterial smooth muscle cell proliferation are mediated by RhoA and Rho-kinase. Circ. Res. *88*, 1102–1104.

Sekine, A., Fujiwara, M., and Narumiya, S. (1989). Asparagine residue in the rho gene product is the modification site for botulinum ADP-ribosyltransferase. J. Biol. Chem. *264*, 8602–8605.

Shi, Q., and King, R.W. (2005). Chromosome nondisjunction yields tetraploid rather than aneuploid cells in human cell lines. Nature *437*, 1038–1042.

Uehata, M., Ishizaki, T., Satoh, H., Ono, T., Kawahara, T., Morishita, T., Tamakawa, H., Yamagami, K., Inui, J., Maekawa, M., and Narumiya, S. (1997). Calcium sensitization of smooth muscle mediated by a Rho-associated protein kinase in hypertension. Nature *389*, 990–994.

Uei, Y., Watanabe, Y., Hirota, T., Yamamoto, H., and Watanabe, H. (1980). Cytologic diagnosis of breast carcinoma with nipple discharge: special significance of the spherical cell cluster. Acta Cytol. *24*, 522–528.

Wang, M., Zhou, X., King, R.W., and Wong, S.T. (2007). Context based mixture model for cell phase identification in automated fluorescence microscopy. BMC Bioinformatics *8*, 32.

Wrobel, C.N., Debnath, J., Lin, E., Beausoleil, S., Roussel, M.F., and Brugge, J.S. (2004). Autocrine CSF-1R activation promotes Src-dependent disruption of mammary epithelial architecture. J. Cell Biol. *165*, 263–273.